Check for updates

BUC-21 coated by NHPI-sensitized ST-01 for enhancing photocatalytic bisphenol A decomposition under low-power visible-light

Chiyao Tang[1] · **Xun Wang**[1] · **Chong-Chen Wang**[1]

Abstract

Within this work, BUC-21/NHPI-ST-01 composites (B1NT*X*) were prepared by facile ball-milling treatment, which displayed better photocatalytic bisphenol A (BPA) decomposition activities under low-power LED visible light than both the individual BUC-21 and NHPI-ST-01. The optimum B1NT3 accomplished 99.4% BPA degradation via photocatalytic treatment within 120 min, which demonstrated satisfied stability and reusability for five successive cycling BPA degradation experiments. The dominant active radicals like $\cdot$OH and $\cdot O_2{}^-$ participated in the BPA decomposition were certificated. The Z-scheme mechanism of photocatalytic BPA degradation over B1NT3 was put forward and affirmed by electrochemical experiment and ESR (electron spin resonance) test. This study suggested the combination of BUC-21 and NHPI-ST-01 was affirmed to be an effective approach for emerging organic pollutants removal.

Keywords BUC-21 · NHPI-sensitized ST-01 · Photocatalysis · Bisphenol A · Degradation

Introduction

Two-dimensional metal-organic frameworks (2D MOFs) have recently attracted widespread research interest due to their fascinating topological networks and entanglements of layered structures [1]. It was believed that 2D MOFs can exhibit better electrical conductivity, higher aspect ratio, more exposed activated sites, faster mass transfer rate and quicker photoinduced charges transfer rate than those

✉ Chong-Chen Wang
wangchongchen@bucea.edu.cn; chongchenwang@126.com

1　Beijing Key Laboratory of Functional Materials for Building Structure and Environment Remediation/Beijing Energy Conservation & Sustainable Urban and Rural Development Provincial and Ministry Co-construction Collaboration Innovation Center, Beijing University of Civil Engineering and Architecture, Beijing 100044, China
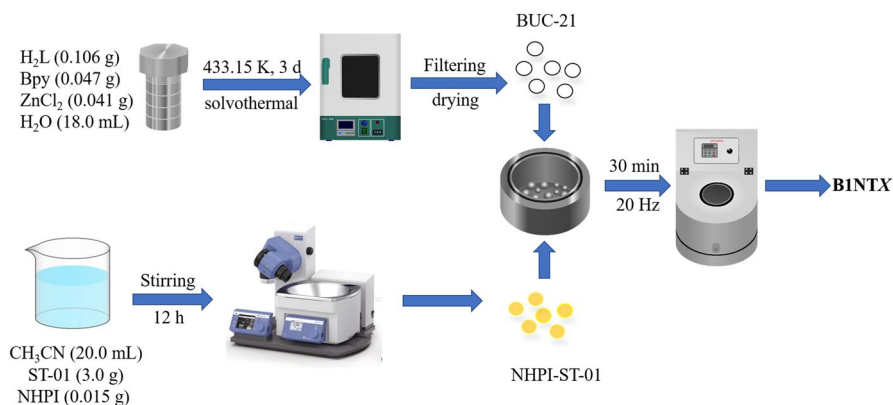
Scheme 1 The preparation illustration of the BUC-21/NHPI-ST-01 (B1NT*X*) composites

of the 3D frameworks [2–4]. BUC-21, as a stable 2D metal-organic framework, was designed and synthesized from *cis*-1,3-dibenzyl-2-oxo-4,5-imidazolidinedicarboxylic acid and Zn^{2+} by our research group, which exhibited outstanding photocatalytic performance toward Cr(VI) reduction and organic pollutant decomposition under UV light [5]. Some visible light responsive semiconductor photocatalysts like g-C_3N_4 [6], N-$K_2Ti_4O_9$ [7], $Bi_{24}O_{31}Br_{10}$ [8], $Cd_{0.5}Zn_{0.5}S$ [9] were introduced to combine with BUC-21 for the purpose of broadening the UV light to the visible light even white light. Also, titanate nanotube (TNT) was adopted as efficient adsorbent for cationic ions to combine with BUC-21 for the construction of adsorbent-photocatalyst composite to accomplish simultaneous Cr(VI) reduction and Cr(III) uptake [6].

As to the construction of MOFs-based composites, our group once published some review papers concerning MOFs/g-C_3N_4 [10], MOF/bismuth-based semiconductor [11] and MOFs/TiO_2 [12]. Especially, the most famous semiconductor photocatalyst TiO_2 nanoparticles with different morphologies displayed different photocatalysis performances [13, 14]. Among different types of TiO_2, the commercial Ishihara ST-01 nanoparticles (anatase TiO_2) were affirmed as the optimal photocatalyst [15]. However, the pristine ST-01 can only be excited by UV light due to its wide band gap [15]. It was deemed that the surface sensitization of nitrogen-containing species can achieve ST-01 to be visible light responsive [16]. For example, Lang and co-workers introduced N-Hydroxyphthalimide (NHPI) to interact with the surficial ·OH groups of ST-01 via covalent bonding for the purpose of oxidizing amine to imines upon the irradiation of visible light [17].

To further overcome the drawback of fast recombination of photo-induced $e^−$-h^+ pairs and improve the photocatalytic efficiency, the NHPI-sensitized ST-01 nanoparticles were coated onto BUC-21 to construct BUC-21/NHPI-ST-01 (B1NT*X*) composites via simple ball-milling method (Scheme 1). BPA, as representative EDCs, have been frequently detected in ambient waterways, which increased their long-term potential toxicity risks to aquatic ecosystems and humans [18]. In this study, the as-prepared B1NT*X* composites were adopted as effective photocatalysts to

decompose BPA under low-power LED visible light. Furthermore, the corresponding photocatalysis mechanism was proposed and tested.

Experimental

Materials and characterization

All reagents were used without any further purification. All the chemicals were of analytical grade, which were used as received without further purification. Anatase TiO_2 (Ishihara Sangyo, ST-01) was purchased from Ishihara Sangyo Kaisha. Ltd., Japan.

The powder X-ray diffraction (PXRD) patterns were recorded on a Dandong-haoyuan DX-2700B diffractometer in the range of $2\theta = 5–80°$. Fourier transform infrared spectra (FTIR) was recorded in the region range from 4000 to 400 cm^{-1} on a Nicolet 6700 infrared spectrophotometer with KBr pellets. High-resolution X-ray photoelectron spectra (XPS) measurement was performed on a Thermo ESCALAB 250XI. UV–visible diffuse-reflectance spectra (UV–vis DRS) of the photocatalysts were recorded from 200 to 800 nm with a Perkin Elmer Lamda 650S spectrophotometer, in which $BaSO_4$ was selected as the standard with 100% reflectance. The transmission electron microscopy (TEM) was observed by JEM 1200EX. Electrochemical measurement was analyzed by Metrohm Autolab PGSTAT204 electrochemical station with 0.2 M Na_2SO_4 solution (initial pH) as the electrolyte in a typical three-electrode mode. The electron spin resonance (ESR) was measured by a JEOL JES-FA200 instrument using 5,5-dimethyl-1-pyrroline-N-oxide (DMPO) as the spin-trapping agent to detect both $\cdot O_2^-$ and $\cdot OH$ radicals. The concentration of the residual BPA was determined by high performance liquid chromatograph (HPLC, Thermo Scientific Vanquish Flex).

Synthesis of BUC-21/NHPI-ST-01 photocatalysts

NHPI-ST-01 was prepared following the method reported by Lang and coworkers [17]. 3.0 g of ST-01 (anatase TiO_2 from Ishihara) was added into 20.0 mL CH_3CN, which was ultrasonicated for 10.0 min to uniformly disperse TiO_2 particles. 0.015 g of N-Hydroxyphthalimide (NHPI) was added into the uniformly dispersed ST-01 in CH_3CN for another 10 min ultrasonication. Afterward, the matrix was stirred for 12 h under dark conditions. Finally, the as-prepared NHPI-ST-01 nanoparticles were separated in a rotary evaporator equipped with a vacuum pump.

BUC-21 was produced solvothermally following the method described by Wang and coworkers [5, 6]. A mixture of $ZnCl_2$ (0.041 g, 0.3 mmol), 4,4′-bipyridine (0.047 g, 0.3 mmol), cis-1,3-dibenzyl-2-imidazolidone-4,5-dicarboxylic acid (0.106 g, 0.3 mmol) and H_2O (18.0 mL) was sealed in a 25.0 mL Teflon-lined

stainless steel pressure vessel, which was heated at 433.15 K for 3 d. The as-obtained BUC-21 particles were separated from the mother aqueous solution via filtration.

The BUC-21/NHPI-ST-01 composites were fabricated by ball-milling the matrix of the as-prepared BUC-21 and NHPI-ST-01 at 30 Hz for 20 min. The obtained BUC-21/NHPI-ST-01 composites with different mass ratios were referred as B1NTX, in which the letters "B" and "NT" are abbreviated as BUC-21 and NHPI-ST-01, respectively. The variable "X" is the mass ratios fraction of NHPI-ST-01 in the composites ($X = 1, 2, 3, 4, 5$).

Photocatalytic performances evaluation of B1NTX composites

The BPA aqueous solution (50.0 mL, initial concentration being 10.0 mg L^{-1}) was chose as pollutant model to evaluate the photocatalysis performances of B1NTX composites (catalyst dosage being 0.4 g L^{-1}) under the irradiation of LED visible light (300 ± 50 mW, PCX50C, Beijing Perfectlight Technology Co., Ltd). After the adsorption-desorption equilibrium was accomplished in 30 min under dark condition, the low-powered LED was used to provide low power visible light to excite the catalyst for BPA degradation. 1.0 mL solution was sampled from the reactor every 30 min to determine the residual BPA concentration on ultra-high performance liquid chromatography equipped with a UV–vis detector and a C18 reversed-phase column (2.1 mm $\times$ 100 mm, 1.7 μm). The mobile phase consisted of acetonitrile and distilled water (50/50, v/v) with the flow rate of 0.40 mL min^{-1} and a column temperature of 40 °C. The injection volume of the filtrate was 20.0 μL, which was tested at the detection wavelength of 227 nm.
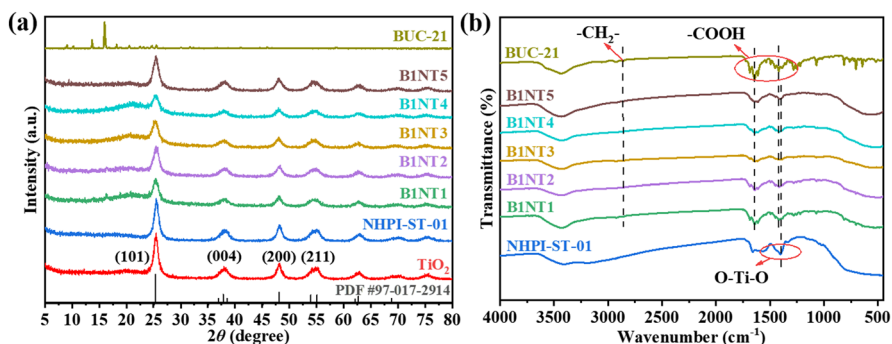

Fig. 1 **a** The PXRD patterns and **b** FTIR spectra of the BUC-21, NHPI-ST-01 and series B1NTX composites

Results and discussion

Characterization of B1NT*X* composites

Figure 1a shows the PXRD patterns of BUC-21, NHPI-ST-01 and series BUC-21/NHPI-ST-01 (B1NT*X*) composites. It was obvious that the diffraction peaks of BUC-21 at 10.2°, 13.6°, 14.8°, 15.9°, 20.5°, 24.5° and 25.5° were perfectly in agreement with related references [5, 6, 9]. As well, the characteristic diffraction peaks at 25.3°, 37.8°, 48.1° and 55.1° corresponded to the (101), (004), (200), and (211) crystal planes of TiO_2 sample[19]. The introduction of NHPI did not alter the anatase phase of ST-01 due to all the diffraction peaks matched perfectly with the standard PXRD patterns (PDF #97-017-2914) [17]. In the PXRD patterns of BUC-21/NHPI-ST-01 (B1NT*X*), the characteristic PXRD peaks of BUC-21 could not be observed obviously due to the excessive NHPI-ST-01 coverage on the BUC-21 surface.

As shown in Fig. 1b, the FTIR peak at 2861 cm^{-1} corresponds to the stretching vibration of υ (–CH_2–) of BUC-21 [6]. A sharp peak at 1402 cm^{-1} can be ascribed to the stretching vibrations of O–Ti–O in NHPI-ST-01 [20]. The strong bands at 1645 and 1417 cm^{-1} are due to the asymmetric and symmetric vibrations of carboxyl groups, respectively [5]. All the characteristic peaks of both BUC-21 and NHPI-ST-01 were observed in the spectra of the B1NT*X* composites, demonstrating the successful fabrication of the B1NT*X* composites.

The construction of electronic interactions can boost the effective interfacial charge transfer between BUC-21 and NHPI-ST-01 [21], in which XPS determination was conducted to explore the possible interactions of the two components in B1NT*X* composites. As illustrated in Fig. 2a, the XPS results depicted that B1NT3 contains Zn, Ti, N and O elements, in which the two obvious Zn 2p and Ti 2p peaks could be attributed to BUC-21 and NHPI-ST-01, respectively. The peaks of Ti $2p_{3/2}$ at 458.8 eV and Ti $2p_{1/2}$ at 464.4 eV affirmed the presence of Ti in the B1NT3 composites [22, 23]. The peaks with binding energies of 1022.37 eV and 1045.37 eV could be ascribed to Zn $2p_{3/2}$ and Zn $2p_{1/2}$
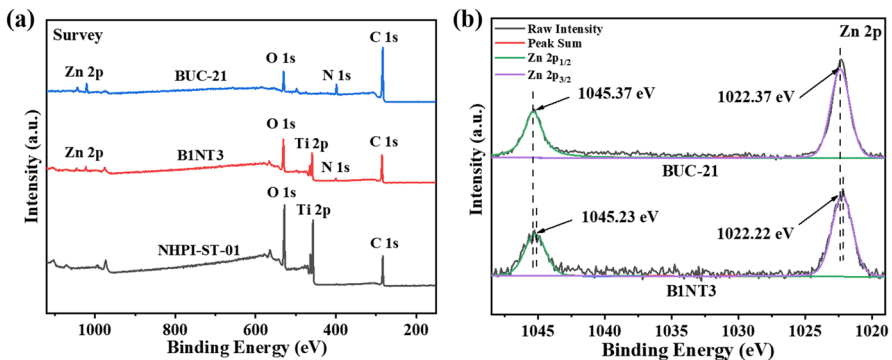

Fig. 2 The XPS spectra of BUC-21, NHPI-ST-01 and B1NT3: **a** survey scan, **b** Zn 2p
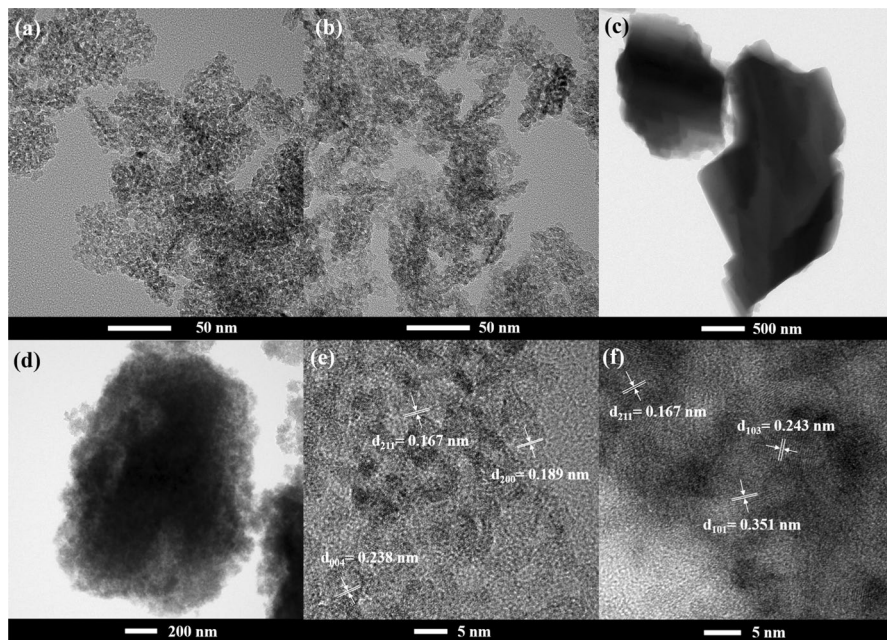
Fig. 3 TEM images of **a** ST-01, **b** NHPI-ST-01, **c** BUC-21 and **d** the optimum B1NT3; HRTEM images of **e** NHPI-ST-01 and **f** B1NT3

of BUC-21, respectively (Fig. 2b) [24]. After the combination of BUC-21 and NHPI-ST-01 (like B1NT3), it was obviously to find that the two peaks at of Zn 2p were shifted from 1022.37 eV and 1045.37 eV in pristine BUC-21 to 1022.22 eV and 1045.23 eV in B1NT3 [25, 26], implying the redistribution of additional electrons in B1NT3 system [27]. And the slight shift of Zn 2p peaks in BUC-21 towards the low binding energy direction further demonstrated the electron transfer from NHPI-ST-01 to BUC-21 after their combination [27].

The morphologies of different samples were observed by TEM and HRTEM. Figure 3a, b depicts that both ST-01 and NHPI sensitized ST-01 demonstrated spherical morphologies with the particle size of 5–7 nm [17]. As well, HRTEM image of NHPI-ST-01 is shown in Fig. 3e. The lattice fringes of 0.167 nm, 0.189 nm and 0.238 nm could be assigned to the (2 1 1), (2 0 0) and (0 0 4) planes of anatase TiO_2 [28–30], indicating that the sensitization process will not affect the morphology and structure of TiO_2. In the TEM and HRTEM images of B1NT3 (Fig. 3d, f), the irregular bulk BUC-21 with particle size of 500–2000 nm was wrapped by the NHPI-ST-01 nano-particles, resulting in ascension of the surface roughness. The calculated lattice spacing of 0.167 nm, 0.243 nm and 0.351 nm were corresponding to (2 1 1), (1 0 3) and (1 0 1) lattice plane of anatase TiO_2 [28, 31, 32], which was consistent with the PXRD results.
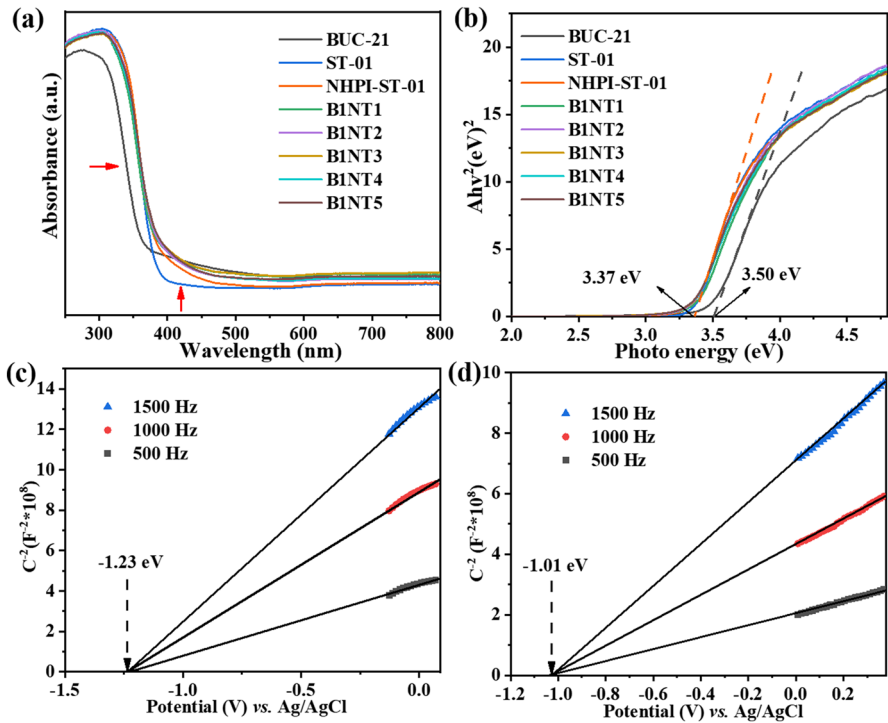
Fig. 4 a The UV–vis DRS spectra and **b** the E_g plots of as-synthesized materials, Mott-Schottky curves of **c** BUC-21 and **d** NHPI-ST-01 at different frequencies

The UV–vis DRS were recorded to explore the optical absorption properties of all BUC-21/NHPI-ST-01 composites. The E_g values (band gap energy) were calculated according to Eq. (1) [33].

$$\alpha h\upsilon = A\left(h\upsilon - E_g\right)^{n/2} \tag{1}$$

where α, h and ν are the diffuse absorption coefficient, the light constant, and the frequency, respectively. In this work, n is 4 due to that B1NT3 is determined as indirect semiconductor [34].

As depicted in Fig. 4a, b, the UV–vis absorption spectra indicated that all the B1NTX composites displayed slight red-shift comparing with that of the individual BUC-21 and NHPI-ST-01. The E_g values of BUC-21, NHPI-ST-01 and B1NT3 were 3.50 eV, 3.37 eV and 3.33 eV, respectively. It was concluded that B1NT3 composites were responsive to the visible light with longer wavelength, which resulted from the formation of visible light absorbing complex [17, 35]. As well, the visible light responsive NHPI-ST-01 contributed to the optical activities of the B1NTX composites, further affirming the interface formed between NHPI-ST-01 and BUC-21 [36].

In addition, the Mott-Schottky measurements were carried out to determine the band position of the conduction band (CB) and charge transfer direction. As

shown in Fig. 4c, d, it can be observed that slope of C^{2-} potential curve of BUC-21 and NHPI-ST-01 was positive, indicating BUC-21 and NHPI-ST-01 were both n-type semiconductors [37].

The flat-band potentials (E_{FB}) of BUC-21 and NHPI-ST-01 were approximately − 1.23 and − 1.01 eV versus the Ag/AgCl electrode, respectively. As to the n-typed semiconductor, the E_{FB} is generally more positive 0.1 eV than the conduction band potential (E_{CB}) [38]. It can be calculated that the lowest unoccupied molecular orbital (LUMO) of BUC-21 and E_{CB} of NHPI-ST-01 were − 1.13 and − 0.91 eV versus NHE, respectively. As well, the highest occupied molecular orbital (HOMO) of BUC-21 and the valence band potential (E_{VB}) of NHPI-ST-01 were calculated to be 2.37 eV and 2.46 eV, respectively, based on the E_g values calculated from UV–vis DRS and the $E_g = E_{VB} − E_{CB}$ equation [6].
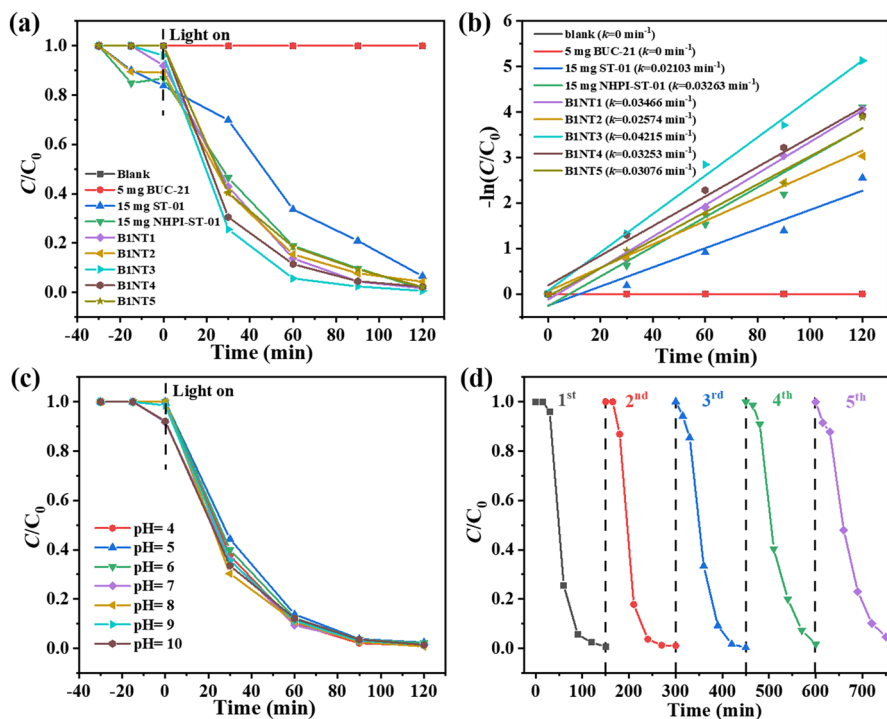

Fig. 5 **a** The photocatalytic degradation efficiencies and **b** degradation rates (*k* values) of BPA over different photocatalysts upon the visible light; **c** The effect of initial pH on degradation of BPA over B1NT3; **d** The recycle of photocatalytic BPA degradation over B1NT3

Table 1 Comparison of photocatalytic BPA degradation activities of various photocatalysts

Catalyst/dosage (mg L^{-1})	Pollutants/mg L^{-1}	Light source	T (min)	Efficiency (%)	References
Cu, N-doped titanate nanotubes/1000	BPA/10	8 W visible light	120	100	[41]
Ce-doped ZnO/800	BPA/10	Sunlight	480	98	[42]
rGO-ZnTi-MMOs/500	BPA/10	300 W Xe arc lamp	180	88	[43]
Ag-ZnO/1000	BPA/10	UV lamp	120	86	[44]
SrTiO$_3$-decorated Ag/AgCl/500	BPA/10	300 W xenon lamp	240	83	[45]
Bi$_{12}$O$_{15}$Cl$_6$ nanosheets/250	BPA/10	350 W Xe arc lamp	360	100	[46]
BiOI/Bi$_2$MoO$_6$/1000	BPA/10	300 W xenon lamp	240	95	[47]
BiVO$_4$/graphene/Bi$_2$O$_3$/1000	BPA/10	150 W metal halide lamp	480	100	[48]
graphene/Bi$_2$Fe$_4$O$_9$/500	BPA/10	150 W Xe arc lamp	180	76	[49]
CNTs/100	BPA/10	150 W xenon	180	75	[50]
BUC-21/NHPI-ST-01/400	BPA/10	300 mW visible light	120	99	This work

Photocatalysis performances of B1NT*X* composites

The photocatalytic BPA degradation performances over different photocatalysts were tested under LED visible light irradiation, in which all B1NT*X* composites demonstrated better photocatalytic performances toward BPA degradation than those of individual BUC-21 and NHPI-ST-01. Especially, the optimal B1NT3 exhibited best BPA degradation activity with decomposition efficiency of 99.4% within 120 min (Fig. 5a). The pseudo-first-order model (ln $[C/C_0] = -kt$) was used to fitted to the kinetic plots of BPA degradation over B1NT*X* composites [39], in which C_0, C and k are the initial BPA concentration, the residual BPA concentration at different time and the reaction rate constant, respectively. The BPA degradation rates (described as k values) over the various photocatalysts followed the order of B1NT3 > B1NT1 > NHPI-ST-01 > B1NT4 > B1NT5 > B1NT2 > ST-01 > BUC-21 (Fig. 5b). Comparing with the photocatalysts reported previously, the B1NT3 composite showed superior photocatalytic BPA degradation activity upon the low-power visible light irradiation in the similar reaction conditions (Table 1).

Generally, the pH of the aqueous solution might heavily influence the photocatalytic activity of the photocatalyst due to that pH can alter the surface charge of the photocatalyst and the species of the targeted organic pollutants [4]. However, in this work, the photocatalytic BPA degradation efficiencies and reaction rates (k values) of B1NT3 maintained at high level under various pH ranging from 4.0 to 10.0, i.e. 99.0%, 97.9%, 97.9%, 98.8%, 99.3%, 98.5% and 98.6% at pH being 4.0, 5.0, 6.0, 7.0, 8.0, 9.0 and 10.0, respectively (Fig. 5c).

Five runs' photocatalytic BPA degradation tests were carried out to check the practical application potential of B1NT3 photocatalyst. The results revealed that the photocatalytic BPA degradation performance of B1NT3 didn't decline noticeably during five runs' usage (Fig. 5d), indicating that B1NT3 photocatalyst was stable and efficient during long-term use.

The identical PXRD patterns and TEM observation further affirmed the stability of B1NT3. The characteristic PXRD peaks at 2θ values of 25.3°, 37.8°, 48.1°and 55.1° were attributed to the (101), (004), (200) and (211) crystal planes of TiO_2
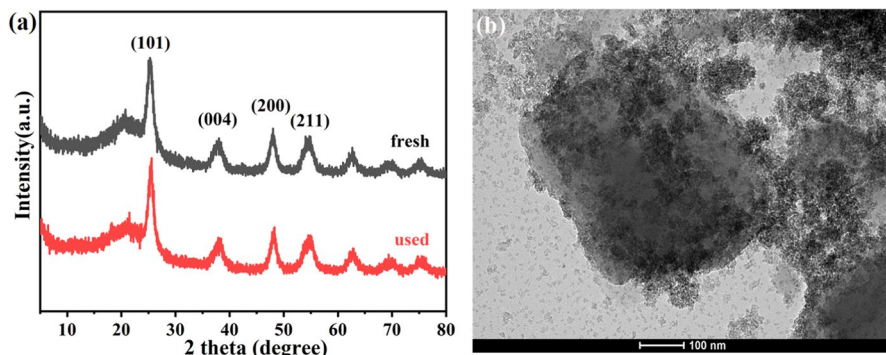

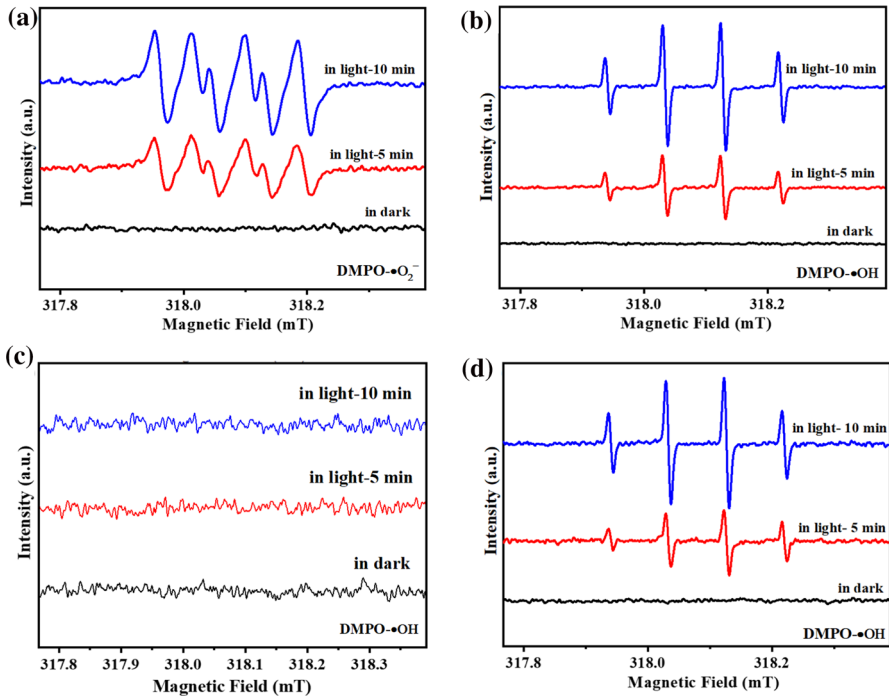**Fig. 6** **a** PXRD pattern and **b** TEM image of B1NT3 after cyclic experiments

Fig. 7 The ESR spectra of **a** DMPO-·O_2^- generated by B1NT3 and DMPO-·OH generated by **b** B1NT3, **c** BUC-21, **d** NHPI-ST-01

[40]. They maintained well indicating that the structure of the B1NT3 composite was hardly affected (Fig. 6a). As well, the TEM images revealed that no noticeable alterations of the morphologies of B1NT3 were observed (Fig. 6b).

Possible formation mechanisms over B1NT*X* composites

The ESR tests can determine the possibly yielded active species over the BUC-21, NHPI-ST-01 and B1NT3 (Fig. 7a–d), which can provide some useful information concerning the major active species to understand the BPA degradation process over B1NT3 and to explore the corresponding photocatalytic mechanism. The ESR signals of ·OH and ·O_2^- with intensity of 1:2:2:1 and 1:1:1:1 were observed over B1NT3 upon visible light irradiation rather than in the dark condition. The corresponding signal intensities became stronger at 10 min's illumination than those at 5 min, affirming that both ·O_2^- and ·OH are yielded due to the photocatalytic reaction. The ·OH signals were detected over the individual NHPI-ST-01 upon the visible light irradiation (Fig. 7d). However, no ·OH signals can be found over the pristine BUC-21 under the identical conditions (Fig. 7c). Due to that the highest occupied molecular orbital (HOMO, 2.37 eV vs. NHE) of BUC-21 was beyond 2.40 eV vs. NHE, the standard potential of the OH⁻/·OH (Fig. 8),
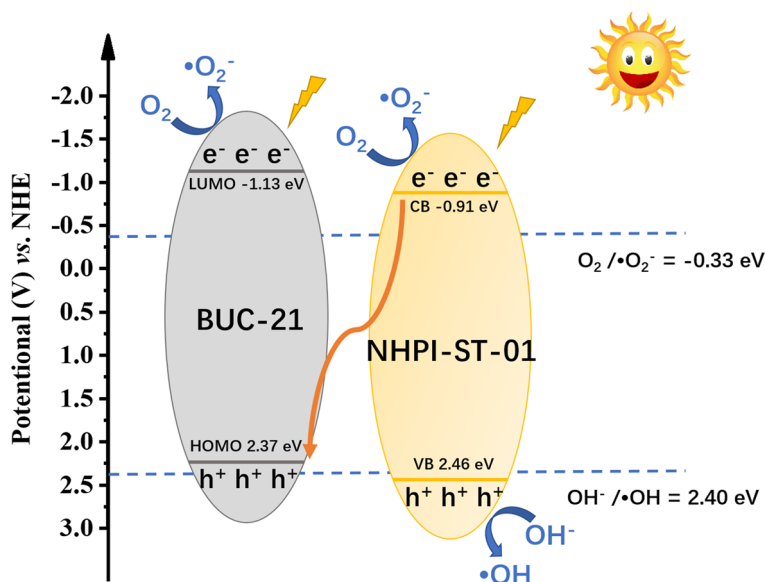
Fig. 8 The possible Z-scheme mechanism of B1NT3 for BPA degradation

the photogenerated h^+ over BUC-21 had no chance to react with OH^-/H_2O to produce the ·OH radicals. However, the h^+ accumulated on the valence band (VB 3.35 eV vs. NHE) of NHPI-ST-01 can oxidize OH^- or H_2O to form ·OH due to the lower position than the $OH^-/·OH$ (2.40 eV vs. NHE) [51].

Based on the above experimental results, the possible Z-scheme mechanism of photocatalytic BPA degradation over B1NT3 was proposed (Fig. 8). Upon the irradiation of visible light, both BUC-21 and NHPI-ST-01 could be excited to form photo-induced holes and electrons (Eq. 2). The photogenerated electrons can migrate from the CB of NHPI-ST-01 to consume holes on the HUMO of BUC-21, which allowed the electrons and holes to accumulate on the LUMO of BUC-21 and VB of NHPI-ST-01, respectively.

Significantly, the LUMO of BUC-21 (-1.13 eV vs. NHE) and CB of NHPI-ST-01 (-0.91 eV vs. NHE) were both much higher than the redox potential of O_2/O_2^- is -0.33 eV vs. NHE [13]. Hence, the dissolved oxygen (DO) molecules can react with the photo-induced e^- to form $·O_2^-$ radicals (Eq. 3) to directly participate in the BPA degradation. Moreover, the position of HUMO of NHPI-ST-01 (2.46 eV vs. NHE) was lower than the redox potential of $OH^-/·OH$ pairs (2.40 eV vs. NHE), the photoinduced h^+ on the surface of NHPI-ST-01 could react with H_2O to produce ·OH (Eq. 4). The possible Z-scheme mechanism can be confirmed by the ESR determination results.

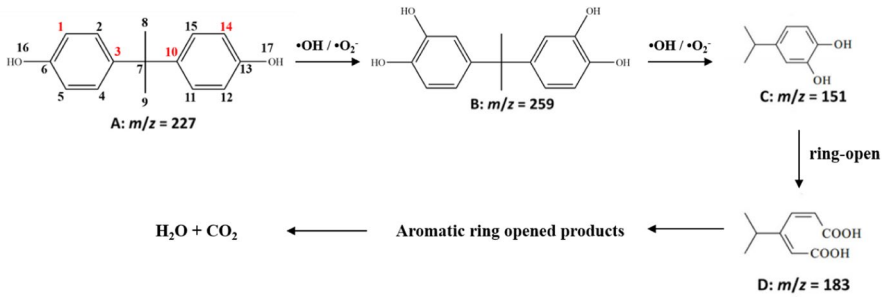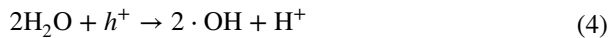$$B1NT3 + light \rightarrow e^- + h^+ \qquad (2)$$

Fig. 9 The proposed pathway for the degradation of BPA

$$O_2 + e^- \rightarrow \cdot O_2^- \tag{3}$$

$$2H_2O + h^+ \rightarrow 2 \cdot OH + H^+ \tag{4}$$

Pathway of BPA degradation

Theoretical DFT was usually used to calculate the Fukui index to determine the potential nucleophilic (f^+) and electrophilic attack (f^-) based on natural population analysis (NPA) charge distribution of BPA molecule, which will further clarify the exact photocatalytic degradation pathways of BPA with the aid the LC-MS measurement [52]. Wang [13] and Liu [53] reported the vulnerable sites of BPA in the presence of free radicals by the Fukui function calculations, in which the C1, C3, C10 and C14 of BPA were the most favorable sites attacked by free radicals like, ·OH and ·O_2^-. According to the results of Fukui function calculation, the possible degradation pathways of BPA by B1NT3 system were proposed, as shown in Fig. 9. Firstly, the ·OH radicals were inclined to attack C1 and C14 sites to yield dihydroxylated BPA (B, m/z=259) [53, 54]. The ·O_2^- radicals preferred to open the aromatic rings with the aid the nucleophilic effect. The C–C bond between the benzene rings was destroyed by both ·OH and ·O_2^- radicals to form intermediate C (m/z=151), which transformed into 2-isopropylmuconic acid (D, m/z=183) via the ring-open reaction. Then, these intermediates might be further decomposed into compounds low molecular weight like short chain aliphatic acids and even completely mineralized to inorganic H_2O and CO_2.

Conclusions

In summary, the BUC-21/NHPI-ST-01 (B1NTX) composites have been successfully fabricated by facile ball-milling treatment. Compared with individual BUC-21 and NHPI-ST-01, B1NTX composites exhibited superior photocatalytic activity on BPA degradation under low-power visible light irradiation, in which the B1NT3 could

degrade ca. 99.4% of BPA under the optimal conditions. Moreover, B1NT3 exhibited effective photocatalytic activity for BPA degradation in a wide pH range from 4.0 to 10.0. The enhanced photocatalytic degradation ability of B1NT3 possibly originated from the different active species like ·OH, and ·O_2^- via direct visible light activation. The corresponding migration pathway of the induced electrons and holes between BUC-21 and NHPI-ST-01 in B1NT3 was proposed by various experiments tests. The cycling tests revealed that the B1NT3 composite was stable and recyclable photocatalyst.

References

1. G. Chakraborty, I.-H. Park, R. Medishetty, J.J. Vittal, Chem. Rev. **121**(7), 3751 (2021)
2. C.-C. Wang, X.-D. Du, J. Li, X.-X. Guo, P. Wang, J. Zhang, Appl. Catal. B. **193**, 198 (2016)
3. A. Dhakshinamoorthy, A.M. Asiri, H. Garcia, Adv. Mater. **31**(41), 1900617 (2019)
4. F.-X. Wang, C.-C. Wang, X. Du, Y. Li, F. Wang, P. Wang, Chem. Eng. J. **429**, 132495 (2022)
5. F.-X. Wang, X.-H. Yi, C.-C. Wang, J.-G. Deng, Chinese J. Catal. **38**(12), 2141 (2017)
6. X.-H. Yi, F.-X. Wang, X.-D. Du, P. Wang, C.-C. Wang, Appl. Organomet. Chem. **33**(1), e4621 (2019)
7. X. Wang, Y.-X. Li, X.-H. Yi, C. Zhao, P. Wang, J. Deng, C.-C. Wang, Chinese J. Catal. **42**(2), 259 (2021)
8. C. Zhao, Z. Wang, X. Li, X. Yi, H. Chu, X. Chen, C.-C. Wang, Chem. Eng. J. **389**, 123431 (2020)
9. X. Wei, P. Wang, H. Fu, C. Zhao, C.-C. Wang, Mater. Res. Bull. **129**, 110903 (2020)
10. C.-C. Wang, X.-H. Yi, P. Wang, Appl. Catal. B. **247**, 24 (2019)
11. C. Zhao, X. Pan, Z. Wang, C.-C. Wang, Chem. Eng. J. **417**, 128022 (2021)
12. C.-C. Wang, X. Wang, W. Liu, Chem. Eng. J. **391**, 123601 (2020)
13. C. Zhao, J. Wang, X. Chen, Z. Wang, H. Ji, L. Chen, W. Liu, C.-C. Wang, Sci. Total Environ. **752**, 141901 (2021)
14. S. Hu, Y. Yu, Y. Guan, Y. Li, B. Wang, M. Zhu, Chin. Chem. Lett. **31**(10), 2839 (2020)
15. H. Xu, J.-L. Shi, S. Lyu, X. Lang, Chinese J. Catal. **41**(10), 1468 (2020)
16. D. Mitoraj, H. Kisch, Angew. Chem. Int. Ed. **47**(51), 9975 (2008)
17. H. Hao, J.-L. Shi, H. Xu, X. Li, X. Lang, Appl. Catal. B. **246**, 149 (2019)
18. D. Fu, Q. Zhang, P. Chen, X. Zheng, J. Hao, P. Mo, H. Liu, G. Liu, W. Lv, RSC Adv. **11**(30), 18308 (2021)
19. S. Saroj, L. Singh, R. Ranjan, S.V. Singh, Res. Chem. Intermed. **45**(4), 1883 (2019)
20. K. Handore, D. Walunj, P. Chhattise, A. Chabukswar, K. Mohite, S. Dallavalle, B. Bharat, V. Chabukswar, Polym. Plast. Technol. Eng. **56**(12), 1259 (2017)
21. J. Ran, B. Zhu, S.Z. Qiao, Angew. Chem. Int. Ed. **56**(35), 10373 (2017)
22. B. Ahmed, D.H. Anjum, M.N. Hedhili, Y. Gogotsi, H.N. Alshareef, Nanoscale **8**(14), 7580 (2016)
23. J. Xi, Y. Zhang, X. Chen, Y. Hu, Res. Chem. Intermed. **46**(4), 2205 (2020)
24. J. Ma, N. Xu, Y. Liu, Y. Wang, H. Li, G. Liu, X. Wang, J. Li, Inorg. Chem. **59**(20), 15495 (2020)
25. Z. Wang, Z. Zhao, L. Zhang, F. Liu, B. Peng, L. Chai, D. Liu, D. Liu, T. Wang, H. Liu, J. Hazard. Mater. **364**, 488 (2019)
26. R. Zhang, Q. Huang, X. Liu, X. Yang, H. Yan, Z. Xiong, N. Xu, J. Ma, Q. Feng, Z. Shen, Mater. Lett. **215**, 173 (2018)
27. J. Ran, X. Wang, B. Zhu, S.-Z. Qiao, Chem. Commun. **53**(71), 9882 (2017)
28. C. Zhang, H. Hua, J. Liu, X. Han, Q. Liu, Z. Wei, C. Shao, C. Hu, Nanomicro. Lett. **9**(4), 1 (2017)

29. K. Zhao, Z. Wu, R. Tang, Y. Jiang, Y. Lu, Res. Chem. Intermed. **41**(7), 4405 (2015)
30. S. Eaimsumang, P. Prataksanon, S. Pongstabodee, A. Luengnaruemitchai, Res. Chem. Intermed. **46**(2), 1235 (2020)
31. J. Zhang, Y. Tian, T. Zhang, Z. Li, X. She, Y. Wu, Y. Wang, J. Wu, ChemCatChem **12**(10), 2760 (2020)
32. P. Verma, S.K. Samanta, Res. Chem. Intermed. **43**(11), 6317 (2017)
33. H. Jia, W. He, B. Zhang, L. Yao, X. Yang, Z. Zheng, Appl. Surf. Sci. **441**, 832 (2018)
34. H. Wang, X. Yuan, Y. Wu, G. Zeng, X. Chen, L. Leng, H. Li, Appl. Catal. B. **174**, 445 (2015)
35. X.-H. Yi, H. Ji, C.-C. Wang, Y. Li, Y.-H. Li, C. Zhao, A. Wang, H. Fu, P. Wang, X. Zhao, Appl. Catal. B. **293**, 120229 (2021)
36. X.-H. Yi, S.-Q. Ma, X.-D. Du, C. Zhao, H. Fu, P. Wang, C.-C. Wang, Chem. Eng. J. **375**, 121944 (2019)
37. L.-P. Sun, S.-Y. Niu, J. Jin, G.-D. Yang, L. Ye, Inorg. Chem. Commun. **9**(7), 679 (2006)
38. X. Jin, L. Ye, H. Wang, Y. Su, H. Xie, Z. Zhong, H. Zhang, Appl. Catal. B. **165**, 668 (2015)
39. Y. Zhang, F. Zhang, Z. Yang, H. Xue, D.D. Dionysiou, J. Catal. **344**, 692 (2016)
40. F. Yang, H. Yang, B. Tian, J. Zhang, D. He, Res. Chem. Intermed. **39**(4), 1685 (2013)
41. R.-A. Doong, C.-Y. Liao, J. Hazard. Mater. **322**, 254 (2017)
42. M. Kamaraj, K.S. Ranjith, R. Sivaraj, R.T. Rajendra Kumar, H.A. Salam, J. Environ. Sci. **26**(11), 2362 (2014)
43. S. Yang, P. Wu, M. Chen, Z. Huang, W. Li, N. Zhu, Y. Ji, RSC Adv. **6**(32), 26495 (2016)
44. A.B. Jasso-Salcedo, G. Palestino, V.A. Escobar-Barrios, J. Catal. **318**, 170–178 (2014)
45. S.-F. Yang, C.-G. Niu, D.-W. Huang, H. Zhang, C. Liang, G.-M. Zeng, Environ. Sci. Nano **4**(3), 585 (2017)
46. C.-Y. Wang, X. Zhang, X.-N. Song, W.-K. Wang, H.-Q. Yu, A.C.S. Appl, Mater. Inter. **8**(8), 5320 (2016)
47. T. Yan, M. Sun, H. Liu, T. Wu, X. Liu, Q. Yan, W. Xu, B. Du, J. Alloys Compd. **634**, 223 (2015)
48. P. Qiu, B. Park, J. Choi, M. Cui, J. Kim, J. Khim, J. Alloys Compd. **706**, 7 (2017)
49. Z.-T. Hu, J. Liu, X. Yan, W.-D. Oh, T.-T. Lim, Chem. Eng. J. **262**, 1022 (2015)
50. J. Qu, Q. Cong, C. Luo, X. Yuan, RSC Adv. **3**(3), 961 (2013)
51. Y. Zhang, J. Zhou, Q. Feng, X. Chen, Z. Hu, Chemosphere **212**, 523 (2018)
52. X.-H. Yi, C.C. Wang, Prog. Chem. **33**(3), 471 (2021)
53. X. Zhao, P. Du, Z. Cai, T. Wang, J. Fu, W. Liu, Environ. Pollut. **232**, 580 (2018)
54. D.P. Subagio, M. Srinivasan, M. Lim, T.-T. Lim, Appl. Catal. B. **95**(3–4), 414 (2010)